


# High-Precise Measurement of Optical Rotatory Dispersion Based on Weak Value Amplification

Jingyi Shao, Lan Luo , Yu He, Jiacheng You, Yurong Liu, Yuyuan Wang, and Zhiyou Zhang

**Abstract**—Chiroptical signals (generally very weak) play significant roles in chiral discrimination that bring great benefits in biochemistry, pharmacy, chemical, and so on. But, high-precise chiroptical detection is still a challenge. In this paper, a high-precise measurement of optical rotatory dispersion (ORD) based on weak value amplification (WVA) is presented. We proposed ORD detection method with parameter separation: by introducing complex coupling strength and dimensionless parameter “intensity contrast ratio” pointer, the ORD is only associated with the imaginary part of the weak value while circular dichroism (CD) is only associated with the real part. By designing a suitable WVA scheme, the ORD and CD can be measured separately. In the experiment, the reliability of the parameter separation method for ORD measurement is verified, and the precision reach the order of  $10^{-6}$  rad. This method has a broad application prospect in biomedical sensing, medicine, chemical analysis and other fields.

**Index Terms**—weak measurement, chiroptical signals, optical rotation, circular dichroism.

## I. INTRODUCTION

CHIRAL molecules, whose mirror images cannot coincide with themselves, always play a significant role in biochemistry, pharmacy, and so on. Existing optical methods for detecting the chiral molecules, such as force chemical microscopy [1], chromatography [2], piezoelectric sensors [3], and fluorescence [4], have their limitations. They either destroy the chiral samples or are complicated to operate. Besides, cavity ring-down polarimetry catch people’s eyes for its high precision on chiral detection recently [5], [6], but it only applies to gas-phase detection and requires a complex instrument. Chiroptical spectroscopy which includes the optical rotatory dispersion (ORD) and circular dichroism (CD) spectra have widely used in chiral detection. ORD refers to the propagation velocity differences between left- and right- circularly polarized light, while CD refers to the differences in absorption of light. The ORD and CD signals are both related to a given wavelength. However, the

Manuscript received June 9, 2021; revised June 27, 2021; accepted June 30, 2021. Date of publication July 7, 2021; date of current version July 29, 2021. This work was supported in part by the Natural Science Foundation of China under Grant 11674234, in part by the Science Specialty Program of Sichuan University under Grant 2020SCUNL210, and in part by the Innovation Project of Sichuan University under Grant 2018SCUH0021. (Corresponding author: Zhiyou Zhang.)

Jingyi Shao, Lan Luo, Yu He, Jiacheng You, Yurong Liu, and Zhiyou Zhang are with the College of Physics, Sichuan University, Chengdu 610064, China (e-mail: 272687088@qq.com; naloul@163.com; 749897850@qq.com; 1138221802@qq.com; 1659692889@qq.com; zhangzhiyou@scu.edu.cn).

Yuyuan Wang is with the Yunnan Institute of Measuring and Testing Technology, Kunming 650228, China (e-mail: 1978449689@qq.com).

Digital Object Identifier 10.1109/JPHOT.2021.3094588

chiroptical signals generally are very weak, although chiroptical spectroscopy is fast response and non-contact, the precision remains limited by using a conventional device.

Recently, a signal enhancement technique called weak value amplification (WVA) makes it possible to solve such a problem. WVA proposed in 1988 by Aharonov, Albert, and Vaidman [7], stepped into the public spotlight for its powerful strength of signal amplification and technical noise suppression [8]–[11]. Therefore, WVA has widely used to measure various physical parameters [12], such as optical spin Hall effect [13]–[17], optical phase [18]–[24], deflection of light beam [25], polarization rotations [9], [26], [27], refractive index variations [28]–[31], magneto-optical constant [32], temporal delays [33]–[35], the layers of graphene [36], optical conductivity of atomically thin crystals [37], single-photon Kerr effect [38], [39] and so on.

More recently, the detection for chiroptical signals based on WVA has also been proposed. Qiu *et al.* proposed a precision method based on weak measurements using the spin Hall effect of light (SHEL) as a probe, and the optical rotatory (OR) angle can be estimated with a precision of 0.2 mdeg [40]. Li *et al.* proposed a high sensitivity scheme for OR estimation based on weak measurement in the frequency domain [41].

However, using SHEL and frequency as probe can only estimate OR in monochromatic light, and chiroptical signals in a wide-band light can reflect more important information of the chiral material, such as the Cotton effect. In addition, the ORD and CD always take place at the same time, and the estimation of an individual ORD (or CD) may lead to inaccurate and incomplete results in actual measurements. Therefore, we proposed a parameter separation method based on WVA for chiroptical signals detection: by introducing complex coupling strength and dimensionless parameter “intensity contrast ratio (ICR)” pointer, the ORD is only associated with the imaginary part of the weak value while CD signal is only associated with the real part by designing a suitable WVA scheme, the ORD and CD can be measured separately. In the experiment, the reliability of parameter separation for ORD measurement is verified, and the precision reach the order of  $10^{-6}$  rad.

## II. THEORETICAL MODEL

A theoretical model for ORD estimation based on WVA is established. We begin with considering the initial polarization state of the system prepared in [20]

$$|\psi_{pre}\rangle = \frac{1}{\sqrt{2}}(|+\rangle + |-\rangle), \quad (1)$$

here,  $|+\rangle = (|H\rangle + i|V\rangle)/2$  and  $|-\rangle = (|H\rangle - i|V\rangle)/2$  denote the left- and right-circularly polarized states, respectively. Where,  $|H\rangle$  and  $|V\rangle$  denote the horizontal and vertical polarization states, respectively.

Then, the beam passes through a chiral sample that interacts differently (i.e. ORD and CD) with left- and right-circularly polarized components. ORD leading to phase variation while CD leading to amplitude variation, which can be expressed by an operator

$$\hat{U} = e^{\frac{i\alpha_\lambda + \theta_\lambda}{2} \hat{A}}, \quad (2)$$

here,  $\alpha_\lambda = 2\pi l(n_L - n_R)/\lambda$  and  $\theta_\lambda = \ln 10(\varepsilon_L - \varepsilon_R)Cl/2$  represent the ORD and CD signals, respectively. Where  $\varepsilon$ ,  $n$ ,  $\lambda$ , and  $C$  are the decadic molar extinction coefficient, refractive index, wavelength, and molar concentration, respectively.  $l$  represents the optical path length (i.e., the thickness of cell).  $\hat{A} = |+\rangle\langle+| - |-\rangle\langle-|$  is the observable of a two-level system. Combining with (1), the state of the whole system evolves into

$$\begin{aligned} |\psi'\rangle &= e^{\frac{i\alpha_\lambda + \theta_\lambda}{2} \hat{A}} |\psi_{pre}\rangle \\ &= \frac{1}{\sqrt{2}} \left( e^{\frac{i\alpha_\lambda + \theta_\lambda}{2}} |+\rangle + e^{-\frac{i\alpha_\lambda + \theta_\lambda}{2}} |-\rangle \right), \end{aligned} \quad (3)$$

here, we consider  $\alpha_\lambda \ll 1$  and  $\theta_\lambda \ll 1$ .

Then, the light beam is post-selected in the polarization states  $|\psi_f\rangle$ , and the intensity of the post-selected light detected in the experiment is given by

$$\begin{aligned} I(\lambda) &= I_0(\lambda) \left| \left\langle \psi_f \left| \exp\left(\frac{i\alpha_\lambda + \theta_\lambda}{2} \hat{A}\right) \right| \psi_{pre} \right\rangle \right|^2 \\ &= I_0(\lambda) \left| \left\langle \psi_f \left| \left( \cos \frac{\alpha_\lambda}{2} + i \hat{A} \sin \frac{\alpha_\lambda}{2} \right) \right. \right. \\ &\quad \left. \left. \times \left( \cosh \frac{\theta_\lambda}{2} + \hat{A} \sinh \frac{\theta_\lambda}{2} \right) \right| \psi_{pre} \right\rangle \right|^2 \\ &\approx I_0(\lambda) |\langle \psi_f | \psi_{pre} \rangle|^2 [1 - \alpha_\lambda \text{Im}(A_w) + \theta_\lambda \text{Re}(A_w)], \end{aligned} \quad (4)$$

where  $A_w = \langle \psi_f | \hat{A} | \psi_{pre} \rangle / \langle \psi_f | \psi_{pre} \rangle$  is weak value which is a complex number. Here,  $I_0(\lambda)$  denotes the initial spectrum of the light without post-selection. In the (4), the approximation is feasible with  $|A_w|^2(\alpha_\lambda^2 + \theta_\lambda^2)/4 \ll 1$ . As shown in (4), the ORD is only associated with the imaginary part of the weak value while CD is only associated with the real part. Therefore, we can adjust the appropriate post-selection to make  $\text{Im}(A_w) \neq 0$  and  $\text{Re}(A_w) = 0$  to measure ORD separately.

To obtain a pure imaginary weak value, we choose the post-selection states as

$$\begin{aligned} \left| \psi_f^\pm \right\rangle &= \frac{1}{\sqrt{2}} [\exp(\mp i\chi) |+\rangle - \exp(\pm i\chi) |-\rangle] \\ &= \frac{1}{\sqrt{2}} i [\sin(\mp\chi) |H\rangle + \cos(\mp\chi) |V\rangle], \end{aligned} \quad (5)$$

here, “ $\pm$ ” denote two symmetry post-selection states concerning the polarization direction being orthogonal to the pre-selection. Where  $\chi \ll 1$  is the post-selected parameters. Therefore, we obtain the weak value as  $A_w^\pm = \mp i \cot \chi$ .

Finally, combining with (4), the intensity of the post-selected light related to the wavelength is obtained with

$$I^\pm(\lambda) \approx I_0(\lambda) \sin^2 \chi [1 - \alpha_\lambda \text{Im}(A_w^\pm)]. \quad (6)$$

The intensity of the post-selected light is reduced by a factor of  $\sin^2 \chi$ , which is the so-called post-selected probability, and the dimensionless parameter “ICR” pointer is introduced to reveal the role of the WVA, which is given by

$$\begin{aligned} \eta(\lambda) &= \frac{I_\delta}{I_{ave}} = \frac{4 \sin \alpha_\lambda |A_w|}{\cos \alpha_\lambda (1 - |A_w|^2) + \cosh \theta_\lambda (1 + |A_w|^2)} \\ &\approx 2\alpha(\lambda) |A_w| = 2\alpha(\lambda) \cot \chi, \end{aligned} \quad (7)$$

here,  $I_\delta = I^+ - I^-$  and  $I_{ave} = (I^+ + I^-)/2$  are the intensities difference and average intensity corresponding to the symmetrical post-selections, respectively. Note that the ICR is proportional to the weak value, which is consistent with the change relationship between the conventional pointer and the weak value. The calculation result of (7) is obtained by linear approximation  $|A_w|^2(\alpha_\lambda^2 + \theta_\lambda^2)/4 \ll 1$ , thus the working points should be located in the linear regime which mentioned in Refs. [20], [42]. Under the linear approximation, a larger ICR can be achieved by choosing a smaller post-selected parameter  $\chi$ . But, when the post-selected parameter  $\chi$  continues to decrease (tending to 0), the above approximation are not valid and the measured region is no longer located in the linear regime.

The intensity of light is the physical quantity being directly measured, so the sources of the technical noise which disturbs the intensity are considered, which is defined as follows

$$I_{noise} \propto \left( \frac{I^+ + I^-}{2} \right)^n, \quad (8)$$

here, we take three types of the technical noise sources in the experimental system into account:  $n = 0$ , indicates the technical noise which is independent of the beam intensity, such as the detector noise and the experimental background noise;  $n = 1/2$ , refers to the shot noise of light (strictly speaking, the shot noise is not the technical noise, but the inherent quantum noise of classical light source);  $n = 1$ , represents the noise proportional to beam intensity, such as the intensity fluctuation caused by laser instability or air turbulence, scattered light due to device imperfect alignment and device defects.

We define the signal-to-noise ratio (SNR) of optical rotation measurement as

$$\begin{aligned} S &= \frac{\partial |I^+ - I^-| / \partial \alpha}{I_{noise}} \delta \alpha \\ &\propto \frac{\partial I_\delta / \partial \alpha}{[(I^+ + I^-) / 2]^n} \delta \alpha, \end{aligned} \quad (9)$$

here,  $\delta \alpha$  is OR variation. When  $n$  is taken to different values, the SNR for the linear response are respectively given by

$$S_{n=0} \propto 2\delta \alpha \sin^2 \chi A_w \approx \delta \alpha \sin 2\chi, \quad (10)$$

$$S_{n=1/2} \propto 2\delta \alpha, \quad (11)$$

$$S_{n=1} \propto 2A_w \delta \alpha \approx 2\delta \alpha \cot \chi. \quad (12)$$

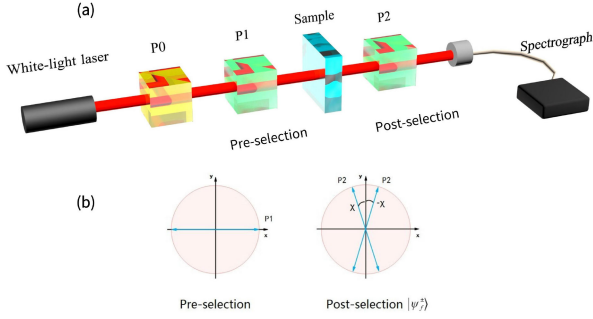


Fig. 1. (a), Experimental setups for the estimation base on weak value amplification: Light source, white light laser; P0, P1 and P2, Glan laser polarizers; Sample, chiral molecule; Spectrograph. (b), the directions of the polarizers for the pre- and post-selection and wave plate.

When only noise of  $n = 0$  is considered, the SNR decreases with the reduction of post-selected parameters  $\chi$ . This is because when the post-selected parameter reduces, the variation of intensity  $I_\delta$  decreases while the noise intensity remains unchanged. When only the scattering noise of light is considered ( $n = 1/2$ ), the SNR is independent of the post-selected parameters  $\chi$ . When only noise of  $n = 1$  is considered, the SNR is proportional to the  $A_w$ . In other words, the WVA effect can obviously improve the SNR.

From the above analysis, it can be concluded that the WVA effect can only suppress the technical noise of  $n = 1$ . For the technical noise of  $n = 0$ , the WVA effect will reduce the measurement precision. However, we can reduce the noise of  $n = 0$  by using low saturation and high sensitivity detector and putting the detector in a nearly enclosed space. Therefore, the main technical noise in the experimental measurement is  $n = 1$ . To conclude, higher precision can be obtained with smaller post-selection parameters for the linear response.

### III. THE EXPERIMENTAL RESULTS

The experiment setups are shown in Fig. 1(a). Glucose solution (right-handed molecule) and fructose solution (left-handed molecule) at different concentrations are selected as samples to measure. A super-continuum laser generated by a white laser (NKT photonics, WL-MICRO), with a 400-1000 nm broadband excitation, passes through a polarizer (P0), which is used to adjust the intensity. Then, the polarizer 1 (P1) is used to prepare the pre-selected state ( $|\psi_{pre}\rangle$ ) with its optical axes placed in the horizontal direction (see Fig. 1(b)). A tiny phase and amplitude variations between the left- and right-circularly polarized state is introduced by the chiral solution in the cuvette (1 cm wide). The post-selected state ( $|\psi_f^\pm\rangle$ ) is prepared by the polarizer 2 (P2), as Fig. 1(b) shown. The optical axis of P2 is rotated  $\chi$  relative to the vertical direction, and the post-selected parameter  $\chi$  is conform to the linear approximation. Finally, the intensity of the post-selected light is recorded by the spectrometer (PG2000-Pro-EX).

The experimental results for ORD estimation are shown in Fig. 2. The concentrations of the glucose and fructose solutions are chosen as  $C=0.01, 0.02, 0.03, 0.04$  g/mL. Figs. 2(a) and

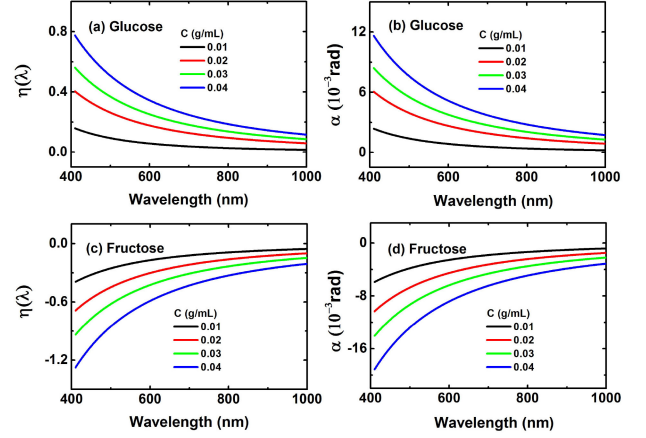


Fig. 2. (a) and (c) show the ICRs  $\eta(\lambda)$  of the samples with different concentrations ( $C = 0.01, 0.02, 0.03, 0.04$  g/mL, respectively). (b) and (d) show the ORD spectra of the samples. The post-selected parameters is chosen as  $\chi = 0.03$  rad.

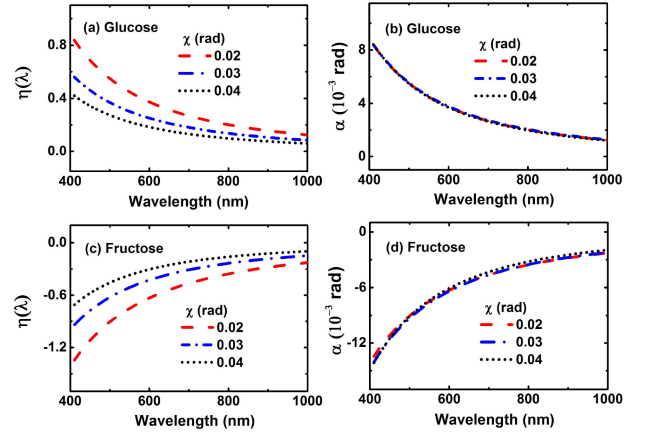


Fig. 3. (a) and (c) show the ICRs  $\eta(\lambda)$  of the samples for different post-selected parameters ( $\chi=0.02, 0.03, 0.04$  rd, respectively). (b) and (d) show the ORD spectra of the samples. The concentrations are both chosen as  $0.03$  g/mL.

(c) show the ICRs  $\eta(\lambda)$  of the glucose and fructose solutions at different concentrations with a fixed post-selected parameter  $\chi = 0.03$  rad, respectively. Note that a larger ICR can be achieved by measuring a higher concentration because the optical rotatory angle  $\alpha_\lambda$  increases with concentration as (13) shown. Besides, the ICRs of the glucose and fructose solutions were the opposite. Thus we can simultaneously determine the magnitude and direction of the chiral molecule. The corresponding optical rotatory angles  $\alpha$  (ORD signal) are calculated according to (7), see Figs. 2(b) and (d).

To further discuss the significance of weak value, we measured the ICRs at different post-selected angles. The post-selected parameter is chosen as  $\chi=0.02, 0.03, 0.04$  rd. The concentrations of glucose and fructose solutions are both  $0.03$  g/mL, corresponding to Figs. 3(a) and (c). It is worth to note that a larger ICR can be achieved by choosing a smaller post-selected parameter on account of weak value amplification as (7) shown. By calculating the ORD (shown in Figs. 3(b) and (d)), we found

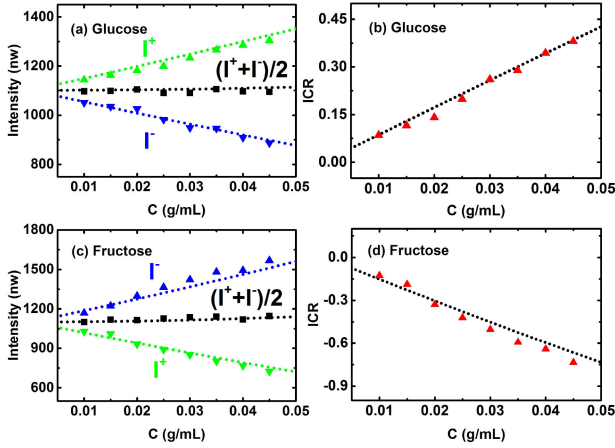


Fig. 4. (a) and (c) show the post-selected intensities of the samples changing with the concentration with the post-selected parameters  $\chi=0.02$  rad, respectively. (b) and (d) show the ICRs of the samples. The lines and dots denote the theoretical predictions and experimental results, respectively.

the same  $\alpha$  can be obtained with different post-selected parameters. This reflects the reliability of the weak value amplification scheme.

To quantitatively analyze the glucose and fructose, we supplement the experiment for measuring optical rotatory angle under monochromatic light. Here, the white laser and the spectrometer are replaced by the He-Ne laser (Thorlabs NL210) with the wavelength of 632.8 nm and CCD (Thorlabs BC106NVIS), respectively. As Fig. 4 shown, the intensity  $I^+$  increases linearly with the increase of the concentration, while  $I^-$  decreases linearly with the increase of the concentration. However, their mean value  $(I^+ + I^-)/2$  has remained almost constant. The magnitude of the ICR is proportional to the concentration. Consistent with the experimental results above, the ICR is positive for the glucose, while it is negative for the fructose.

The specific rotation is expressed by the following formula [40]

$$[\alpha] = \frac{\alpha}{lC}, \quad (13)$$

here,  $l$  is the thickness of the cell.  $C$  is the concentration of sample. Therefore, we obtain the specific rotation of glucose and fructose as  $49^\circ$  and  $-81^\circ$  at the 632.8 nm wavelength from the numerical fitting results. Refer to the previous work [40], the rationality of the scheme is confirmed.

Finally, we discuss the measurement precision of the optical rotation angle  $\alpha$ , which could be estimated by using the  $\Delta\alpha = \Delta I_\delta / [\partial(I^+ - I^-) / \partial\alpha]$ . Here,  $\Delta I_\delta$  represents the standard deviations of the phase according to the experimental measurements and  $\partial I_\delta / \partial\alpha$  represents the sensitivity. In our experiment, the sensitivity we obtained is  $2.04 \times 10^5$  nW/rad. The standard deviations was calculated as a order of 1 nW. Therefore, we obtain the precision of the order of  $10^{-6}$  rad.

We further analyze the variation trend of the measurement precision with the concentration. Figs. 5(a) and (b) show that the average intensity ( $I_{ave}$ ) is basically unchanged. The intensity difference ( $I_\delta$ ) increases with the increase of the concentration,

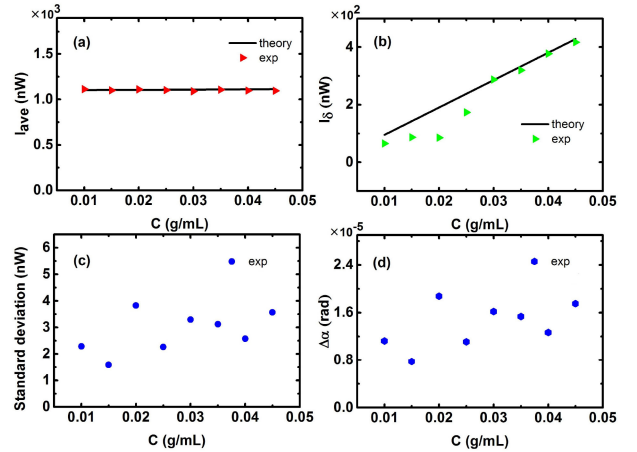


Fig. 5. (a) and (b) show the intensities ( $I_{ave}$  and  $I_\delta$ ) of the post-selected light changing with the concentrations; Dots and solid lines denote experiment results and theoretical prediction, respectively. (c) show the intensity standard deviation. (d) show the precision of the experiment. The post-selected parameters are chosen as  $\chi = 0.02$  rad.

because  $I_\delta$  is equal to the change in intensity caused by the concentrations. Figs. 5(c) and (d) show the intensity standard deviation and precision. With the change of concentration, the standard deviation and precision are basically maintained in a specific range.

#### IV. CONCLUSION

To conclude, we have established a theoretical model based on WVA for the ORD signals estimations. In the experiment, the ORD signals under visible light of the glucose and fructose solutions with different concentrations were determined. The reliability of the parameter separation method for ORD measurement is verified, and the precision reach the order of  $10^{-6}$  rad. These results provide a sample and precision method of the chiroptical characterization and analysis, which may have important applications in life science, pharmacy, and even materialogy.

#### ACKNOWLEDGMENT

The authors declare no conflicts of interest.

#### REFERENCES

- [1] R. Mckendry, M. E. Theoclitou, T. Rayment, and C. Abell, "Chiral discrimination by chemical force microscopy," *Nature*, vol. 391, no. 6667, pp. 566–568, 1998.
- [2] B. Chankvetadze, "Recent developments on polysaccharide-based chiral stationary phases for liquid-phase separation of enantiomers," *J. Chromatogr. A*, vol. 1269, no. SI, pp. 26–51, 2012.
- [3] K. Bodenhofer, A. Hierlemann, J. Seemann, G. Gauglitz, B. Koppenhoefer, and W. Gopel, "Chiral discrimination using piezoelectric and optical gas sensors," *Nature*, vol. 387, no. 1–2, pp. 577–580, 1997.
- [4] T. James, K. Sandanayake, and S. Shinkai, "Chiral discrimination of monosaccharides using a fluorescent molecular sensor," *Nature*, vol. 374, no. 6520, pp. 345–347, 1995.
- [5] M. Thomas, K. B. Wiberg, and P. H. Vaccaro, "Cavity ring-down polarimetry (CRDP): A new scheme for probing circular birefringence and circular dichroism in the gas phase," *J. Phys. Chem. A*, vol. 104, no. 25, pp. 5959–5968, 2000.

- [6] D. Sofikitis, L. Bougas, G. E. Katsoprinakis, A. K. Spiliotis, B. Loppinet, and T. P. Rakitzis, "Evanescence-wave and ambient chiral sensing by signal-reversing cavity ringdown polarimetry," *Nature*, vol. 514, no. 7520, pp. 76–79, 2014.
- [7] Y. Aharonov, D. Z. Albert, and L. Vaidman, "How the result of a measurement of a component of the spin of a spin-1/2 particle can turn out to be 100," *Phys. Rev. Lett.*, vol. 60, no. 14, pp. 1351–1354, 1988.
- [8] D. J. Starling, P. B. Dixon, A. N. Jordan, and J. C. Howell, "Optimizing the signal-to-noise ratio of a beam-deflection measurement with interferometric weak values," *Phys. Rev. A*, vol. 80, no. 4, p. 041803, 2009.
- [9] N. W. M. Ritchie, J. G. Story, and R. G. Hulet, "Realization of a measurement of a "weak value"," *Phys. Rev. Lett.*, vol. 66, no. 9, pp. 1107–1110, 1991.
- [10] D. J. Starling, P. B. Dixon, A. N. Jordan, and J. C. Howell, "Precision frequency measurements with interferometric weak values," *Phys. Rev. A*, vol. 82, no. 6, pp. 27938–27954, 2010.
- [11] Y. Kedem, "Using technical noise to increase the signal-to-noise ratio of measurements via imaginary weak values," *Phys. Rev. A*, vol. 85, no. 6, pp. 121–125, 2012.
- [12] G. Jayaswal, G. Mistura, and M. Merano, "Weak measurement of the Goos-Hänchen shift," *Opt. Lett.*, vol. 38, no. 8, pp. 1232–1234, 2013.
- [13] O. Hosten and P. Kwiat, "Observation of the spin hall effect of light via weak measurements," *Science*, vol. 319, no. 5864, pp. 787–790, 2008.
- [14] S. Chen, X. Zhou, C. Mi, H. Luo, and S. Wen, "Modified weak measurements for the detection of the photonic spin hall effect," *Phys. Rev. A*, vol. 91, no. 6, p. 062105, 2015.
- [15] X. Zhou, Z. Xiao, H. Luo, and S. Wen, "Experimental observation of the spin hall effect of light on a nano-metal film via weak measurements," *Phys. Rev. A*, vol. 85, no. 4, p. 043809, 2011.
- [16] G. Jayaswal *et al.*, "Observation of the Imbert-Fedorov effect via weak value amplification," *Opt. Lett.*, vol. 39, no. 8, pp. 2266–2269, 2014.
- [17] Y. He *et al.*, "Periodically manipulating the photonic spin hall effect with an electric field," *Appl. Phys. Exp.*, vol. 12, no. 9, p. 092009, 2019.
- [18] X. Xu, Y. Kedem, K. Sun, L. Vaidman, C. Li, and G. Guo, "Phase estimation with weak measurement using a white light source," *Phys. Rev. Lett.*, vol. 111, no. 3, p. 033604, 2013.
- [19] L. Li *et al.*, "Phase amplification in optical interferometry with weak measurement," *Phys. Rev. A*, vol. 97, no. 3, p. 033851, 2018.
- [20] X. Qiu *et al.*, "Precision phase estimation based on weak-value amplification," *Appl. Phys. Lett.*, vol. 110, no. 7, p. 071105, 2017.
- [21] L. Luo *et al.*, "Simultaneously precise estimations of phase and amplitude variations based on weak-value amplification," *Appl. Phys. Lett.*, vol. 114, no. 11, p. 111104, 2019.
- [22] C. Li, X. Xu, J. Tang, J. Xu, and G. Guo, "Ultrasensitive phase estimation with white light," *Phys. Rev. A*, vol. 83, no. 4, p. 044102, 2011.
- [23] C. Fang, J. Huang, Y. Yu, Q. Li, and G. Zeng, "Ultra-small phase estimation via weak measurement with postselection: A comparison of joint weak measurement and weak value amplification," *J. Phys. B: Atom. Mol. Opt. Phys.*, vol. 49, p. 175501, 2015.
- [24] N. Brunner and C. Simon, "Measuring small longitudinal phase shifts: Weak measurements or standard interferometry?," *Phys. Rev. Lett.*, vol. 105, no. 1, p. 010405, 2010.
- [25] P. B. Dixon, D. J. Starling, A. N. Jordan, and J. C. Howell, "Ultrasensitive beam deflection measurement via interferometric weak value amplification," *Phys. Rev. Lett.*, vol. 102, no. 17, pp. 173601–173601, 2009.
- [26] B. de Lima S. Bernardo Azevedo, and A. Rosas, "Ultrasensitive polarization rotation measurements via weak value amplification," *Phys. Lett. A*, vol. 378, no. 30–31, pp. 2029–2033, 2014.
- [27] B. de Lima Bernardo, S. Azevedo, and A. Rosas, "Weak value amplified optical activity measurements," *Opt. Exp.*, vol. 19, no. 17, pp. 16508–16517, 2011.
- [28] L. Xu, L. Luo, H. Wu, Z. Luo, and H. Cui, "Ultrasensitive optical refractive index detection of NaCl and alcohol solutions based on weak value amplification," *Plasmonics*, vol. 15, no. 2, pp. 671–678, 2019.
- [29] L. Luo, X. Qiu, L. Xie, X. Liu, and J. Du, "Precision improvement of surface plasmon resonance sensors based on weak-value amplification," *Opt. Exp.*, vol. 25, no. 18, pp. 21107–21114, 2017.
- [30] Y. Zhang, D. Li, Y. He, Z. Shen, and Q. He, "Optical weak measurement system with common path implementation for label-free biomolecule sensing," *Opt. Lett.*, vol. 41, no. 22, p. 5409, 2016.
- [31] X. Zhou, L. Sheng, and X. Ling, "Photonic spin hall effect enabled refractive index sensor using weak measurements," *Sci. Rep.*, vol. 8, no. 1, p. 1221, 2018.
- [32] X. Qiu *et al.*, "Determination of magneto-optical constant of Fe films with weak measurements," *Appl. Phys. Lett.*, vol. 105, no. 13, p. 131111, 2014.
- [33] L. J. Salazar-Serrano, D. Janner, N. Brunner, V. Pruneri, and J. P. Torres, "Measurement of sub-pulse-width temporal delays via spectral interference induced by weak value amplification," *Phys. Rev. A*, vol. 89, no. 1, p. 012126, 2013.
- [34] G. Struebi and C. Bruder, "Measuring ultrasensitive time delays of light by joint weak measurements," *Phys. Rev. Lett.*, vol. 110, no. 8, p. 083605, 2013.
- [35] F. Chen, J. Huang, Y. Yang, Q. Li, and G. Zeng, "Ultra-small time-delay estimation via a weak measurement technique with post-selection," *J. Phys. B: At. Mol. Phys.*, vol. 49, no. 17, p. 175501, 2016.
- [36] X. Zhou, X. Ling, H. Luo, and S. Wen, "Identifying graphene layers via spin hall effect of light," *Appl. Phys. Lett.*, vol. 101, no. 25, p. 251602, 2012.
- [37] S. Chen, X. Ling, W. Shu, H. Luo, and S. Wen, "Precision measurement of the optical conductivity of atomically thin crystals via the photonic spin hall effect," *Phys. Rev. Appl.*, vol. 13, no. 1, p. 014057, 2020.
- [38] G. Chen *et al.*, "Achieving heisenberg-scaling precision with projective measurement on single photons," *Phys. Rev. Lett.*, vol. 121, no. 6, pp. 060506.1–060506.7, 2018.
- [39] G. Chen, N. Aharon, Y. N. Sun, Z. H. Zhang, and G. C. Guo, "Heisenberg-scaling measurement of the single-photon Kerr non-linearity using mixed states," *Nature Commun.*, vol. 9, no. 1, p. 93, 2018.
- [40] X. Qiu, L. Xie, X. Liu, L. Luo, Z. Zhang, and J. Du, "Estimation of optical rotation of chiral molecules with weak measurements," *Opt. Lett.*, vol. 41, no. 17, p. 4032, 2016.
- [41] D. Li *et al.*, "Optical rotation based chirality detection of enantiomers via weak measurement in frequency domain," *Appl. Phys. Lett.*, vol. 112, no. 21, p. 213701, 2018.
- [42] A. G. Kofman, S. Ashhab, and F. Nori, "Nonperturbative theory of weak pre- and post-selected measurements," *Phys. Rep.*, vol. 520, no. 2, pp. 43–133, 2011.